DISCONTINUOUS BIFURCATION ANALYSIS OF COUPLED RATE-DEPENDENT PLASTICITY AND DAMAGE

Wenqing Hu and Zhen Chen
Department of Civil and Environmental Engineering
University of Missouri-Columbia, Columbia, MO 65211-2200, USA

ABSTRACT

The transition from continuous to discontinuous failure modes during the dynamic failure evolution can be identified by performing discontinuous bifurcation analysis. As can be found from the open literature, however, a continuum tangent stiffness tensor has not been formulated for coupled rate-dependent plasticity and damage in model-based simulation of dynamic fracture and damage events. Based on the previous work [1,2], a thermodynamically consistent framework is established in this study for coupled rate-dependent plasticity and damage models, via which rate-dependent Drucker-Prager plasticity coupled with isotropic damage is formulated with model parameters being calibrated from SHPB (Split Hopkins Pressure Bar) experiments. To identify the transition from continuous to discontinuous failure modes, discontinuous bifurcation analysis is performed based on the rate-dependent continuum tangent stiffness tensor that is derived from the coupled plasticity/damage model. To develop a robust model-based simulation procedure, a geometric criterion with a corresponding solution scheme is presented to investigate the localized failure condition in the Mohr coordinates. According to the experimental data available, the uniaxial compressive loading path is considered to illustrate the loading rate effect on the critical localization orientation and hardening parameters. It is shown that the higher the loading rate, the later discontinuous bifurcation would occur in the loading path. It appears from this study that the coupled rate-dependent plasticity/damage model could be combined with a decohesion model for multi-scale simulation of failure evolution involving different degrees of discontinuity, without invoking higher-order spatial terms in the stress-strain space.

1 INTRODUCTION

In contrast to the dominance of microcracking in tension [1], quasi-brittle solids under impact loading exhibit a drastically different behavior in compression, for which two dominant modes of irreversible changes, i.e., plastic flow and microcracks, exist. It requires a coupled rate-dependent plasticity and damage model. However, the boundary value problem for a local continuum of strain-softening features becomes ill-conditioned resulting in instabilities. As can be found from the open literature, two different kinds of approaches have been proposed over the last twenty years to model and simulate the evolution of localized material failure, namely, continuous and discontinuous ones. Smeared crack approach, non-local models, viscous or gradient regularized models, etc. are among the continuous approaches proposed to regularize the localization problems, in which the higher order terms in space and/or time are introduced into the stress-strain relations so that the mathematical model is well-posed in a higher order sense for given boundary and/or initial data. On the other hand, decohesion and fracture mechanics models are representative of discontinuous approaches, in which strong discontinuities are introduced into a continuum body such that the governing differential equation is well posed for given boundary and/or initial data. Since the discontinuous bifurcation identifies the transition from continuous to discontinuous failure modes [2-4, among others], it appears that a combined rate-dependent local damage/plasticity and decohesion approach could be sound in physics and efficient in computation. However, it is necessary to find an efficient way to determine the critical hardening parameters and critical localization orientations with the discontinuous bifurcation analysis. The key to perform the discontinuous bifurcation analysis is to formulate an acoustic tensor, which is obtained by contracting the continuum tangent stiffness tensor with the normal vector of eventual localization band [5]. With the aid of a very attractive geometric representation of the localization condition in

the Mohr strain/stress coordinates, the missing information on the transition between failure modes of different discontinuities and the type of material failure could be obtained without using a tedious numerical algorithm [6-8].

In this paper, a continuum tangent stiffness tensor for the rate-dependent Drucker-Prager plasticity coupled with isotropic damage is introduced first. In order to bridge the gap between rate-dependent continuous and discontinuous failure modes in impact problems, a geometric criterion in the Mohr coordinates is presented next to investigate the localized failure condition for the coupled rate-dependent plasticity and damage model. For the purpose of illustration, the loading rate effect on the critical localization orientation and critical hardening parameters is studied for uniaxial compressive loading path with model parameters being calibrated from SHPB (Split Hopkins Pressure Bar) experiments. Conclusions are given in the final section.

2 A COUPLED RATE-DEPENDENT PLASTICITY AND DAMAGE MODEL

With the use of the "equivalent strain principle" and "effective stress principle", a thermodynamically consistent framework for a coupled rate-dependent plasticity and damage model has been developed for quasi-brittle materials under impact loading, with a focus on compressive responses. The "effective-stress" is the essential mechanism by which theories of elastoplasticity are coupled with damage theories. In the "effective-stress" space $\hat{\boldsymbol{\sigma}}$, the fourth-order stiffness tensor $\mathbf{E}^e \equiv \partial\hat{\boldsymbol{\sigma}}/\partial\boldsymbol{\varepsilon}^{\mathrm{e}}$ with $\boldsymbol{\varepsilon}^{\mathrm{e}}$ being truly elastic strain. In the actual stress space $\boldsymbol{\sigma}$, the fourth order stiffness tensor $\hat{\mathbf{E}}^e \equiv \partial\boldsymbol{\sigma}/\partial\boldsymbol{\varepsilon}^e$ and damage related stress tensor $\boldsymbol{\beta} \equiv -\partial\boldsymbol{\sigma}/\partial d$ with d being a scalar damage variable. By introducing the suitable yield function Φ and the dissipative potential Φ^*, the continuum tangent stiffness tensor can be derived as

$$\hat{\mathbf{T}}^{ep} = \hat{\mathbf{E}}^e - \frac{1}{h}\left(\hat{\mathbf{E}}^e : \boldsymbol{\varphi}^* + C_d\boldsymbol{\beta}\right)\otimes\boldsymbol{\varphi} : \mathbf{E}^e \tag{1}$$

where $\boldsymbol{\varphi} \equiv \partial\Phi/\partial\hat{\boldsymbol{\sigma}}$, $\boldsymbol{\varphi}^* \equiv \partial\Phi^*/\partial\hat{\boldsymbol{\sigma}}$ and $h = \boldsymbol{\varphi} : \mathbf{E}^e : \boldsymbol{\varphi}^* + H$ with H being the hardening modulus. Notice that C_d is a monotonically increasing scalar function of the strain rate and the equivalent damage strain $\tilde{\varepsilon}_{equ} = \sqrt{\sum(\langle\varepsilon_i\rangle^+)^2}\,/3.0$ with ε_i being the *ith* component of the principal strain tensor and $\langle x\rangle^+$ being the positive part of x.

As a special case of the general theory, consider a rate-dependent Drucker-Prager plasticity model coupled with isotropic damage. Here the yield function is defined as

$$\Phi(\hat{\boldsymbol{\sigma}}, K) = \hat{\tau}_e + \alpha\hat{I}_1 - (\eta\sigma_y - K) \tag{2}$$

with η being the strain rate sensitivity function, σ_y the yield strength under quasi-static uniaxial compressive loading, K the hardening stress, and α the coefficient of pressure effect. Notice that in Eqn (2) the equivalent effective stress $\hat{\tau}_e = \sqrt{\frac{3}{2}\hat{\mathbf{s}} : \hat{\mathbf{s}}} \Rightarrow \partial\hat{\tau}_e/\partial\hat{\boldsymbol{\sigma}} = \sqrt{\frac{3}{2}}\,\hat{\mathbf{s}}\big/\sqrt{\hat{\mathbf{s}} : \hat{\mathbf{s}}}$ with $\hat{\mathbf{s}}$ being the deviatoric stress in the "effective-stress" space and the first invariant in the "effective-stress" space $\hat{I}_1 = \hat{\sigma}_{ii}$. A nonassociated flow rule of von Mises type is chosen to be

$$\Phi^*(\hat{\boldsymbol{\sigma}}, K) = \hat{\tau}_e - (\eta\sigma_y - K). \tag{3}$$

Similar to the second invariant in the actual stress space $J_2 = \frac{1}{2}\mathbf{s} : \mathbf{s}$, we use $\hat{J}_2 = \frac{1}{2}\hat{\mathbf{s}} : \hat{\mathbf{s}}$ in the "effective-stress" space. Because of $\mathbf{s} = (1-d)\hat{\mathbf{s}}$, $J_2 = (1-d)^2\hat{J}_2$ and $I_1 = (1-d)\hat{I}_1$, we obtain from Eqn (2) that

$$\boldsymbol{\varphi} = \frac{\partial\Phi}{\partial\hat{\boldsymbol{\sigma}}} = \sqrt{\frac{3}{2}}\frac{\hat{\mathbf{s}}}{\sqrt{\hat{\mathbf{s}} : \hat{\mathbf{s}}}} + \alpha\boldsymbol{\delta} = \sqrt{\frac{3}{2}}\frac{\mathbf{s}}{\sqrt{\mathbf{s} : \mathbf{s}}} + \alpha\boldsymbol{\delta} = \frac{\sqrt{3}}{2}\frac{\mathbf{s}}{\sqrt{J_2}} + \alpha\boldsymbol{\delta}, \tag{4}$$

and from Eqn (3) that

$$\boldsymbol{\varphi}^* = \frac{\partial\Phi^*}{\partial\hat{\boldsymbol{\sigma}}} = \sqrt{\frac{3}{2}}\frac{\hat{\mathbf{s}}}{\sqrt{\hat{\mathbf{s}} : \hat{\mathbf{s}}}} = \sqrt{\frac{3}{2}}\frac{\mathbf{s}}{\sqrt{\mathbf{s} : \mathbf{s}}} = \frac{\sqrt{3}}{2}\frac{\mathbf{s}}{\sqrt{J_2}}. \tag{5}$$

By introducing $\boldsymbol{\sigma} = (1-d)\hat{\boldsymbol{\sigma}}$, the stiffness tensor in the actual stress space becomes

$$\hat{\mathbf{E}}^e = (1-d)\mathbf{E}^e = 2G\left(\frac{\dot{\bar{\varepsilon}}}{\bar{\varepsilon}}\right)(1-d)\left(\mathbf{I}_4 + \frac{\upsilon}{1-2\upsilon}\boldsymbol{\delta}\otimes\boldsymbol{\delta}\right), \tag{6}$$

where υ is Poisson's ratio that is taken to be rate-independent. Finally $\boldsymbol{\beta}$ is defined as

$$\boldsymbol{\beta} \equiv -\frac{\partial \boldsymbol{\sigma}}{\partial d} = \hat{\boldsymbol{\sigma}} = \frac{\boldsymbol{\sigma}}{1-d}\,. \tag{7}$$

With the use of the above equations, it follows from Eqn (1) that the continuum tangent stiffness tensor takes the form of

$$\hat{\mathbf{T}}^{ep} = (1-d)\mathbf{E}^e - \frac{1}{h}\left((1-d)\mathbf{E}^e : \frac{\sqrt{3}}{2}\frac{\mathbf{s}}{\sqrt{J_2}} + C_d\frac{\boldsymbol{\sigma}}{1-d}\right)\otimes\left(\frac{\sqrt{3}}{2}\frac{\mathbf{s}}{\sqrt{J_2}} + \alpha\boldsymbol{\delta}\right) : \mathbf{E}^e \tag{8}$$

for the rate-dependent Drucker-Prager plasticity coupled with isotropic damage.

3 GEOMETRICAL LOCALIZATION ANALYSIS IN THREE DIMENSIONS

Once the tangent operators for quasi-brittle materials are established, failure in the small, that is, failure at the constitutive level, may be analyzed. The possibility of jumps in the velocity field is detected by the singularity of the acoustic tensor. Assuming plastic-damage loading persists on both sides of the discontinuity surface, the acoustic tensor for the coupled rate-dependent plasticity and damage model can be obtained by contracting the continuum tangent stiffness tensor $\hat{\mathbf{T}}^{ep}$ given by Eqn (8) with the vector $\mathbf{n}$ normal to the discontinuity surface, namely,

$$\hat{\mathbf{Q}}^{ep} = \mathbf{n}\cdot\hat{\mathbf{T}}^{ep}\cdot\mathbf{n} = \hat{\mathbf{Q}}^{e} - \frac{1}{h}\mathbf{a}^*\otimes\mathbf{a} \tag{9}$$

where the pre-conditioner $\hat{\mathbf{Q}}^e = \mathbf{n}\cdot\hat{\mathbf{E}}^e\cdot\mathbf{n}$ denotes the acoustic tensor of linear elasto-damage. The so-called traction vectors of elastoplastic-damage bifurcation in Eqn (9) are $\mathbf{a} = \boldsymbol{\varphi} : \mathbf{E}^e\cdot\mathbf{n}$ and $\mathbf{a}^* = \mathbf{n}\cdot\left(\hat{\mathbf{E}}^e : \boldsymbol{\varphi}^* + C_d\boldsymbol{\beta}\right)$. If the acoustic tensor is singular, i.e., $\det\hat{\mathbf{Q}}^{ep} = 0$, spatial discontinuities may develop in the form of jumps in the velocity field.

In order to analyze the bifurcation condition, we form the generalized eigenvalue problem $\mathbf{B} = \left(\hat{\mathbf{Q}}^e\right)^{-1}\cdot\hat{\mathbf{Q}}^{ep}$ as proposed by Ottosen and Runesson [5]. It can be found that $\mathbf{B} = \boldsymbol{\delta} - 1/h\left(\hat{\mathbf{Q}}^e\right)^{-1}\cdot\mathbf{a}^*\otimes\mathbf{a}$, which is a rank-one tensor with two of the three eigenvalues (λ_1, λ_2, λ_3) being one. Since $\mathbf{B}$ is a rank-one tensor, it follows that $\det\mathbf{B} = \lambda_1\lambda_2\lambda_3 = 0$, i.e., the remaining unknown eigenvalue is equal to zero. By performing the trace operation of $\mathbf{B}$, we can find that $tr(\mathbf{B}) = \lambda_1 + \lambda_2 + \lambda_3 = tr(\boldsymbol{\delta}) - h^{-1}\left(\hat{\mathbf{Q}}^e\right)^{-1} : (\mathbf{a}^*\otimes\mathbf{a})$. Hence, the bifurcation condition may be represented in terms of a function of $\mathbf{n}$, namely,

$$\det\mathbf{B} = \frac{\det\hat{\mathbf{Q}}^{ep}}{\det\hat{\mathbf{Q}}^{e}} = 1 - \frac{1}{h}Y(\mathbf{n}) = 0\,, \tag{10}$$

where $Y(\mathbf{n}) = \mathbf{a}(\mathbf{n})\cdot\hat{\mathbf{P}}^{e}(\mathbf{n})\cdot\mathbf{a}^*(\mathbf{n})$ with $\hat{\mathbf{P}}^{e}(\mathbf{n}) = \left(\hat{\mathbf{Q}}^{e}\right)^{-1}$. In other words, the bifurcation condition Eqn (10) takes the form of

$$H + \boldsymbol{\varphi} : \mathbf{E}^{e} : \boldsymbol{\varphi}^* - Y(\mathbf{n}) = 0\,, \tag{11}$$

which provides the critical hardening modulus H^{crit} at incipient localization as H reaches the maximum value for all possible orientations $\mathbf{n} = \mathbf{n}(\theta)$.

From Eqns (4) and (6), the traction vector $\mathbf{a}$ reads

$$\mathbf{a} = \boldsymbol{\varphi} : \mathbf{E}^e\cdot\mathbf{n} = 2G\left(\frac{\sqrt{3}}{2}\frac{\mathbf{s}\cdot\mathbf{n}}{\sqrt{J_2}} + \frac{1+\upsilon}{1-2\upsilon}\alpha\mathbf{n}\right). \tag{12}$$

From Eqns (5-7), the traction vector $\mathbf{a}^*$ reads

$$\mathbf{a}^* = \mathbf{n}\cdot\left(\hat{\mathbf{E}}^e : \boldsymbol{\varphi}^* + C_d\boldsymbol{\beta}\right) = \left(G\sqrt{3}(1-d)\frac{\mathbf{s}\cdot\mathbf{n}}{\sqrt{J_2}} + C_d\frac{\mathbf{s}\cdot\mathbf{n}}{1-d} + C_d\frac{I_1}{3(1-d)}\mathbf{n}\right). \tag{13}$$

In the case of isotropic damage, the elasto-damage acoustic tensor $\hat{\mathbf{Q}}^e$ and its inverse may be evaluated analytically as follows:

$$\hat{\mathbf{Q}}^e = \mathbf{n}\cdot\hat{\mathbf{E}}^e\cdot\mathbf{n} = G(1-d)\left(\boldsymbol{\delta} + \frac{1}{1-2\upsilon}\mathbf{n}\otimes\mathbf{n}\right) \tag{14}$$

with $\mathbf{n}\cdot\mathbf{I}_4\cdot\mathbf{n} = \boldsymbol{\delta}/2 + 1/2\,\mathbf{n}\otimes\mathbf{n}$, and the inverse of $\hat{\mathbf{Q}}^e$ from Eqn (14) takes the form of

$$\hat{\mathbf{P}}^e = \frac{1}{G(1-d)}\left(\boldsymbol{\delta} - \frac{1}{2(1-\upsilon)}\mathbf{n}\otimes\mathbf{n}\right). \tag{15}$$

Thus the hardening modulus can be found from Eqn (11) as

$$H = \mathbf{a}\cdot\hat{\mathbf{P}}^e\cdot\mathbf{a}^* - \boldsymbol{\varphi} : \mathbf{E}^e : \boldsymbol{\varphi}^*. \tag{16}$$

Because of $\mathbf{n}\cdot\mathbf{s}\cdot\mathbf{n} = \mathbf{n}\cdot\boldsymbol{\sigma}\cdot\mathbf{n} - I_1/3 = \sigma_N - I_1/3$ and $(\mathbf{s}\cdot\mathbf{n})\cdot(\mathbf{s}\cdot\mathbf{n}) = \tau_N^2 + (\mathbf{n}\cdot\mathbf{s}\cdot\mathbf{n})^2$, we may recast the localization condition Eqn (16) with Eqns (4-5), (12-13), and (15) into

$$\frac{(\sigma_N - \sigma_0)^2}{A^2} + \frac{\tau_N^2}{B^2} = 1\,, \tag{17}$$

where $\sigma_0 = \dfrac{I_1}{3} - \dfrac{\alpha(1+\upsilon)}{2\omega(1-2\upsilon)} - \dfrac{\gamma}{2\xi}$ $A^2 = (H+3G)\dfrac{(1-d)(1-\upsilon)}{(1-2\upsilon)\omega\xi} + \left(\dfrac{\alpha(1+\upsilon)}{2\omega(1-2\upsilon)} - \dfrac{\gamma}{2\xi}\right)^2$, and $B^2 = \dfrac{1-2\upsilon}{2(1-\upsilon)}A^2$,

in which we define $\omega \equiv \dfrac{\sqrt{3}}{2\sqrt{J_2}}$, $\xi \equiv 2G\omega(1-d) + \dfrac{C_d}{1-d}$, and $\gamma \equiv \dfrac{C_d I_1}{3(1-d)}$. This condition forms an ellipse in the $\sigma_N - \tau_N$ space of Otto Mohr [8].

For a given stress state, we can evaluate the Mohr components σ_N and τ_N in order to check the bifurcation condition, Eqn (17), via the Mohr envelope concept [8]. Let the principal stress circle be represented by

$$(\sigma_N - \sigma_c)^2 + \tau_N^2 = R^2\,, \tag{18}$$

where the radius $R = (\sigma_1 - \sigma_3)/2$ with $\sigma_1 \ge \sigma_2 \ge \sigma_3$, and the center $\sigma_c = (\sigma_1 + \sigma_3)/2$. The critical hardening parameter H^{crit} and the critical failure angle θ^{crit} can then be obtained when the major principal circle of stress osculates the localization ellipse, namely, by solving Eqns (17) and (18) simultaneously. This yields the critical failure angle as

$$\tan^2\theta^{cri} = \frac{1-\cos 2\theta}{1+\cos 2\theta} = \frac{R - (1-2\upsilon)(\sigma_c - \sigma_0)}{R + (1-2\upsilon)(\sigma_c - \sigma_0)}. \tag{19}$$

Correspondingly, the bifurcation may take place when the hardening modulus reaches the critical value, namely,

$$H^{cri} = \frac{(1-2\upsilon)\omega\xi}{(1-d)(1-\upsilon)}\left(\frac{2(1-\upsilon)}{1-2\upsilon}R^2 + 2(1-\upsilon)(\sigma_c - \sigma_0)^2 - \left(\frac{\alpha(1+\upsilon)}{2\omega(1-2\upsilon)} - \frac{\gamma}{2\xi}\right)^2\right) - 3G\,. \tag{20}$$

4 GEOMETRICAL SOLUTION UNDER UNIAXIAL COMPRESSIVE STRESS

In the previous section, a generalized geometrical solution for localization in three dimensions has been derived based on the continuum tangent stiffness tensor for coupled rate-dependent Drucker-Prager plasticity with isotropic damage. Let us now consider the relations that are related to the uniaxial compressive stress state, which is defined by $\sigma_{11} = \sigma_{22} = 0$ and $\sigma_{33} < 0$. For this case, the

Table 1: Critical Localization Parameters

strain rate	290 /s	620 /s	1050 /s	1500 /s
bifurcation point (σ_{33})	-37.96 (MPa)	-19.24 (MPa)	-9.60 (MPa)	-7.22 (MPa)
failure angle	41.6°	41.6°	41.6°	41.6°
damage	0.31	0.75	0.91	0.96

radius $R = -\sigma_{33}/2$ and the center of the Mohr circle $\sigma_c = \sigma_{33}/2$. Under the uniaxial compressive loading path, the difference between H from the actual stress state and H^{crit} from Eqn (20) is checked at each time step. If $\left|H - H^{cri}\right| \le tol$, a small positive tolerance parameter, then bifurcation occurs, compute the critical failure angle from Eqn (19); otherwise, continue to next step.

With the above procedure, we examine the failure modes involved in the SHPB laboratory experiments as simulated in [9]. Table 1 shows the critical localization parameters under different strain rates along the uniaxial compressive loading path. Figure 1 depicts geometrical contact conditions between the localization ellipse and the major stress circle of Mohr at the strain rate of 620/s. As can be seen, localization occurs only if the material exhibits damage. With the increase of strain rate, the bifurcation point falls deeper in the post peak regime. It is interesting to note that the failure angles under different strain rates are constant for the coupled rate-dependent plasticity and damage model, which is consistent with the previous study using a rate-independent Drucker-Prager plasticity model combined with a rate-dependent tensile damage model [3]. To verify the analytical results, a numerical bifurcation study is performed at the constitutive level. As shown in Fig. 2, the localization diagram plots the normalized determinant $\det \hat{\mathbf{Q}}^{ep} / \det \hat{\mathbf{Q}}^{e}$ for in-plane failure angles ranging from $0° < \theta < 180°$ at the strain rate of 620 /s. The zero values of the normalized localization determinant verify the analytical/geometrical localization results using the Mohr envelope concept.

5 CONCLUSIONS

In this paper, a generalized geometric criterion with a corresponding solution scheme is presented to investigate the localized failure conditions in the Mohr coordinates, based on the rate-dependent continuum tangent stiffness tensor for the coupled rate-dependent Drucker-Prager plasticity with isotropic damage. For the purpose of illustration, critical localization orientations and critical hardening parameters are studied for the uniaxial compressive stress loading path under

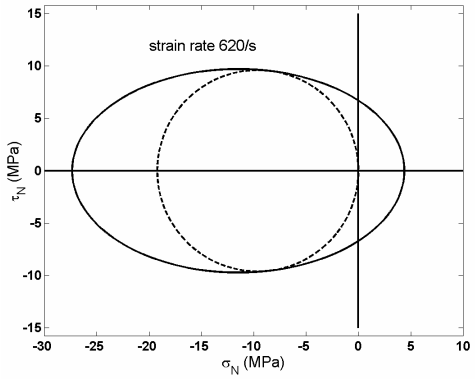

Figure 1: Localization ellipse and Mohr's circle for strain rate of 620/s.

different strain rates. In contrast to the insensitivity of critical localization orientation to the strain rate, the strong loading rate effect on the bifurcation stress state is particularly noteworthy. To the author's knowledge, it is the first time to find that the increase of loading rate would decrease the bifurcation point in the post-peak regime. By identifying the transition from continuous to discontinuous failure modes, the coupled rate-dependent plasticity and damage model could be combined with a decohesion model for large-scale simulation of failure evolution without invoking higher-order spatial terms in the stress-strain space. An integrated experimental, analytical and numerical effort is required to further verify the solution procedure proposed here.

Acknowledgement
This research was partially supported by US-NSF and CHINA-NSF.

References:

[1] Chen, Z., Hu, W., and Chen, E. P. "Simulation of dynamic failure evolution in brittle solids without using nonlocal terms in the strain-stress space." CMES-Computer Modeling in Engineering & Sciences. 1(4), 57-62, 2000.
[2] Chen, Z. "Continuous and discontinuous failure modes." Journal of Engineering Mechanics-ASCE. 122(1), 80-82, 1996.
[3] Chen, Z., Deng, M., and Chen, E. P. "Rate-dependent transition from tensile damage to discrete fracture in dynamic brittle failure." Theoretical and Applied Fracture Mechanics. 35(3), 229-235, 2001.
[4] Chen, Z., and Hu, W. "On the continuous and discontinuous approaches for simulating localized damage." Proceedings of the International Workshop on Bifurcations & Instabilities in Geomechanics, IWBI 2002, A.A. BALKEMA PUBLISHERS, Minneapolis MN, USA, 2002.
[5] Ottosen, N. S., and Runesson, K. "Properties of discontinuous bifurcation solutions in elastoplasticity." International Journal of Solids & Structures. 27(4), 401-421, 1991.
[6] Pijaudier-Cabot, G., and Benallal, A. "Strain localization and bifurcation in a non-local continuum." International Journal of Solids & Structures. 30, 1761-1775, 1993.
[7] Rizzi, E., Carol, I., and Willam, K. "Localization analysis of elastic degradation with application to scalar damage." Journal of Engineering Mechanics-ASCE. 121(4), 541-554, 1995.
[8] Liebe, T., and Willam, K. "Localization properties of generalized Drucker-Prager elastoplasticity." Journal of Engineering Mechanics-ASCE. 127(6), 616-619, 2001.
[9] Grote, D. L., Park, S. W., and Zhou, M. "Dynamic behavior of concrete at high strain rates and pressures: I. experimental characterization." International Journal of Impact Engineering. 25(9), 869-886, 2001.

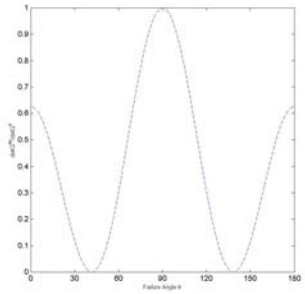

Figure 2: Verification of the analytical bifurcation results at the strain rate of 620 /s.